

Traversable ℓ -wormholes supported by ghost scalar fields

Belen Carvente,^{1,*} Víctor Jaramillo,^{1,†} Juan Carlos Degollado,^{2,‡} Darío Núñez,^{1,§} and Olivier Sarbach^{3,¶}

¹*Instituto de Ciencias Nucleares, Universidad Nacional Autónoma de México,
Circuito Exterior C.U., A.P. 70-543, México D.F. 04510, México*

²*Instituto de Ciencias Físicas, Universidad Nacional Autónoma de México,
Apdo. Postal 48-3, 62251, Cuernavaca, Morelos, México*

³*Instituto de Física y Matemáticas, Universidad Michoacana de San Nicolás de Hidalgo,
Edificio C-3, Ciudad Universitaria, 58040 Morelia, Michoacán, México*

(Dated: October 31, 2019)

We present new, asymptotically flat, static, spherically symmetric and traversable wormhole solutions in General Relativity which are supported by a family of ghost scalar fields with quartic potential. This family consists of a particular composition of the scalar field modes, in which each mode is characterized by the same value of the angular momentum number ℓ , yet the composition yields a spherically symmetric stress-energy-momentum and metric tensor. For $\ell = 0$ our solutions reduce to wormhole configurations which had been reported previously in the literature. We discuss the effects of the new parameter ℓ on the wormhole geometry including the motion of free-falling test particles.

PACS numbers: 04.20.q, 04.20.Jb, 04.40.b

I. INTRODUCTION

The essential property of General Relativity, namely, that matter determines the geometry of the spacetime, acquires a new light when the matter is such that it violates the energy conditions [1–5]. In particular, the violation of the null energy condition opens the possibility for the existence of globally hyperbolic, asymptotically flat spacetimes with non-trivial topological structures [6]. Such matter, usually referred to as *exotic* in the literature, generates peculiar responses in the properties of the spacetime curvature with important consequences on the effective gravitational potential, producing potential “bumps” instead of the usual potential wells. To provide an explicit example, in Fig. 1, we present the gravitational effective potentials for a massive, radially infalling test particle for two cases: the first one is due to the presence of a point mass which generates the usual gravitational well, whereas the second one is generated by a distribution of exotic matter (as the one discussed later in this work) in which case the potential exhibits a different type of convexity corresponding to a gravitational potential bump.

*belen.carvente@correo.nucleares.unam.mx

†victor.jaramillo@correo.nucleares.unam.mx

‡jcdegollado@icf.unam.mx

§nunez@nucleares.unam.mx

¶sarbach@ifm.umich.mx

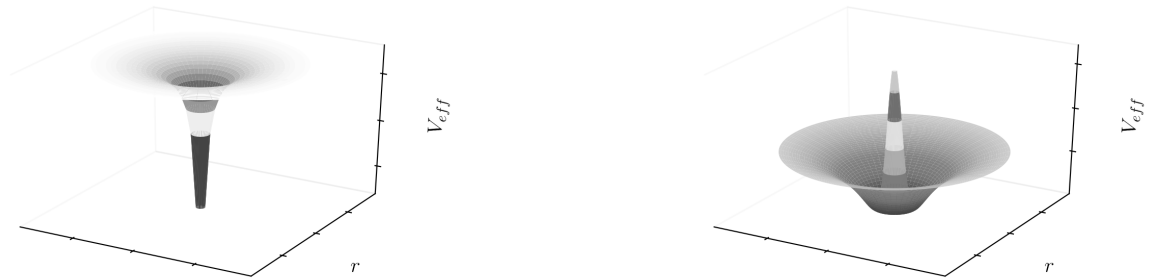


FIG. 1: Gravitational potential produced by a point mass $\sim -1/r$ (left panel) and by the exotic distribution presented in this work (right panel), see section V A. In both cases a test particle with vanishing angular momentum is considered.

Moreover, under specific circumstances, the *bump* could be such that it connects two separated regions of spacetime. The resulting configuration is dubbed *wormhole*, and it offers challenges and opportunities to better understand the relation between matter and geometry, aside from the fact that, being bona fide solutions to Einstein’s equations, it could potentially describe an astrophysical scenario if exotic matter turns out to actually being present in our Universe.

In cosmology, matter with negative pressure can be used to describe the observed accelerated expansion of the Universe [7–10] and seems to be favored by several observational constraints [11–13]. Additionally, modeling the dark energy with an equation of state of the form $p = \omega\rho$, the observations suggest a value of ω close to -1 or even smaller, in which case the existence of astrophysical or cosmological wormholes becomes plausible.

The studies of traversable wormholes have their origin with Ellis’ work [14], where the author presented a black hole like solution to Einstein’s equations, and in order to remove the singularity, used a scalar field and *drain the hole*. Actually, the same solution, based on a different approach was obtained almost at the same time by Bronnikov [15]. It turned out that the solution represented a bridge between two regions of the spacetime [16]. Over the years, the idea was further developed, and the best known example of a traversable wormhole appeared in 1988, in the work of Morris and Thorne [17]. Since then, a plethora of literature has arisen and the complexity of the models has increased, see for example [18, 19] and references therein.

In order to obtain a wormhole solution to the Einstein equations, some works use generation procedures, such as the Newman-Janis algorithm, which allows to obtain a Kerr black hole solution starting from a Schwarzschild one; in this way, a rotating (although not asymptotically flat) solution was obtained starting from one of the original Ellis models [20]. There is also a technique which uses the thin shell approach, which assumes that the matter is concentrated in a three-dimensional submanifold. However, a common practice is to analyze the geometry describing a putative wormhole without mentioning the possible matter that could generate it, artificially producing general forms of such wormholes which might even include rotation [21]; in the words of Morris and Thorne: fixed the geometry... “and let the builders of a wormhole synthesize, or search throughout the universe for, materials or fields with whatever stress-energy tensor might be required” [17].

In the present work, we prefer to avoid this “reversed engineering approach” and assume the specification of a suitable matter model which allows for a large class of static, spherically symmetric and traversable wormhole solutions. In particular, following the recent approach in [22] to construct a generalized class of static and spherically symmetric boson stars, we consider a family of massive, complex and self-interacting ghost scalar fields similar to the one considered in Dzhunushaliev *et al.* [23, 24], but which includes an extra parameter ℓ mimicking the effects of the angular momentum. In this way, new spherical and traversable wormhole solutions can be constructed which generalize those of Refs. [23, 24] to $\ell > 0$. Accordingly, and following the terminology of the ℓ -boson stars, we dub these solutions ℓ -wormholes.

While Ellis’ original solutions use a massless, time-independent real scalar field without self-interaction, in this work we consider massive, complex and self-interacting scalar fields with a harmonic time-dependency *à la* Dzhunushaliev *et al.* [23, 24], but instead of considering just a single field we consider a family of fields with angular momentum number ℓm with ℓ fixed and $m = -\ell, \dots, \ell$. Assuming like in [22] that each of these fields has exactly the same radial dependency, we obtain static, spherically symmetric wormhole solutions. When $\ell = 0$, the mass of the scalar field, its self-interaction and the time-frequency vanish one recovers Ellis’ wormhole solutions.

The new wormholes have several interesting characteristics, such as curvature scalars and effective potentials which

smooth out the features of the corresponding 0-wormholes. The geodesic motion helps us to understand the role played by the ℓ -parameter in the spacetime configuration. Finally, the presence of a new parameter gives rise to the possibility that this wormhole might be stable, a feature that will be discussed in a followup work.

The paper is organized as follows. In Section II, we specify our metric ansatz describing static, spherical symmetric and traversable wormhole spacetimes and introduce the matter model. In Section III, we derive the static field equations in spherical symmetry, discuss some qualitative properties of the wormhole solutions and then construct numerical solutions to the field equations whose main properties are discussed next in Section IV. In Section V, we discuss the embedding diagrams visualizing the spatial geometry of the solutions, derive the geodesic equations for massive or massless test particles propagating in the wormhole metric and analyze the motion under several conditions determined by the wormhole parameters. Finally, we discuss and summarize our results in Section VI.

II. FOUNDATIONS

The determination of the stress-energy-momentum tensor that supports a wormhole geometry is of the utmost importance to understand its physical properties and structure. As already mentioned in the introduction, an asymptotically flat wormhole geometry in general relativity requires the matter to be *exotic*, that is, matter that does not fulfill the regular properties of the usual matter we deal with everyday.¹ More specifically, the matter must violate the null energy condition, $T_{\mu\nu}k^\mu k^\nu \geq 0$, where $T_{\mu\nu}$ is the stress-energy-momentum tensor and k^μ any null vector [17, 19, 27]. Incidentally, this is also the fundamental ingredient of the so-called ghost energy, a model not excluded by observations to be a candidate for dark energy. For instance, constraints from the Supernovae Ia Hubble diagram [28] favor the existence of an equation of state for such dark fluid, $p = \omega\rho$ with $\omega < -1$, a model consistent with ghost energy [4].

In practice, violation of the null energy condition is accomplished by changing the global sign in the stress-energy-momentum tensor in Einstein's equations. Ellis called this the *other polarity of the equations* [14]. This change in sign in the equations is attributed to the type of matter, and has multiple implications which might lead to misunderstandings. A global change in sign to the stress-energy-momentum tensor implies that the usual definition of density also has the opposite sign and is thus negative.

In this work we interpret the physical properties of the wormhole directly in terms of the theory of general relativity and Einstein's field equations, so that the exotic matter produces a different reaction in the curvature of the spacetime, particularly in the effective potential in which the test particles move, generating bumps instead of wells, so that a particle has to spend potential energy in order to get closer to the source, while it gains kinetic energy and accelerates when getting away from it; like when climbing a mountain to reach the summit and then going down.

In particular, we stress that when talking about test particles we assume the validity of the weak equivalence principle, which assumes that the inertial and gravitational masses are equal to each other. Therefore, free-falling test particles or photons always follow causal geodesics of the underlying spacetime, regardless of the sign of their mass.² The ‘‘bump interpretation’’ mentioned so far will become evident when analyzing the geodesic motion of test particles in Section V.

A. Metric ansatz

We will consider a static spherically symmetric spacetime with a line element of the form:

$$ds^2 = -a(r) c^2 dt^2 + a(r)^{-1} dr^2 + R^2(r) d\Omega^2, \quad (2.1)$$

where R and a are positive functions only of the radial coordinate r , and $d\Omega^2 = d\theta^2 + \sin^2\theta d\varphi^2$. Notice that for $R^2 = r^2 + b^2$, with b a positive constant, and $a = 1$, the reflection-symmetric Ellis wormhole metric is recovered [14] and, from it, with a suitable redefinition of the radial coordinate, one obtains the usual form of the Morris–Thorne like wormhole [17]. Also note that the coordinate r our work is based on extends from $-\infty$ to $+\infty$, and we will demand that R be regular at the throat $r = 0$, which corresponds to a minimum of the area $4\pi R^2$ of the invariant two-spheres.

¹ However, it should be mentioned that there are examples of traversable wormholes without exotic matter in modified theories of gravity [25] or in general relativity when the asymptotic flatness condition is replaced by adS-asymptotics [26].

² However, see [29] for bizarre implications in systems involving hypothetical point particles with positive and negative masses.

B. Matter content

In the present work, we consider a set of several massive scalar fields with a self-interaction term. Our configurations are constructed in such a way that the sum of the fields preserves the spherical symmetry of the stress-energy-momentum tensor and includes an extra parameter associated with the angular momentum number ℓ . This approach was introduced in [30] in the context of critical collapse, and recently used in [22] to construct ℓ -boson stars.

We start with the Lagrangian density for N complex massive scalar fields

$$\mathcal{L}_\Phi = -\frac{1}{2\kappa} \left[\sum_{i=1}^N \eta \nabla_\mu \Phi_i \nabla^\mu \Phi_i^* + V(|\Phi|^2) \right], \quad (2.2)$$

with a quartic potential

$$V(|\Phi|^2) = \sum_{i=1}^N V^{(i)} = \sum_{i=1}^N \left(\eta_\mu \frac{m_\Phi^2 c^2}{\hbar^2} |\Phi_i|^2 + \eta_\lambda \frac{\lambda}{2\hbar^2} |\Phi_i|^2 \sum_{j=1}^N |\Phi_j|^2 \right) \quad (2.3)$$

where $\kappa = 8\pi G/c^4$, \hbar is the reduced Planck constant, m_Φ is the mass of the scalar field particle and λ is the parameter measuring the strength of the quartic interaction term. The values $\eta = \eta_\mu = \eta_\lambda = 1$ represent the canonical scalar fields while $\eta = \eta_\mu = -\eta_\lambda = -1$ describe the type of ghost fields in which we will be interested in, and from now on we fix the latter choice. In the following, for convenience, we will work with the rescaled quantities $\mu = m_\Phi c/\hbar$ and $\Lambda = \lambda/2\hbar^2$ instead of m_Φ and λ .

The stress-energy-momentum tensor associated with the scalar field Φ_i is thus given by

$$T_{\mu\nu}^{(i)} = \frac{c^4}{16\pi G} \left[-(\nabla_\nu \Phi_i \nabla_\mu \Phi_i^* + \nabla_\nu \Phi_i \nabla_\mu \Phi_i^*) - g_{\mu\nu} \left(-\nabla_\alpha \Phi_i \nabla^\alpha \Phi_i^* + V^{(i)} \right) \right], \quad (2.4)$$

while the total stress-energy-momentum tensor that we plug into Einstein's field equations is

$$T_{\mu\nu} = \sum_{i=1}^N T_{\mu\nu}^{(i)}. \quad (2.5)$$

In [30], for the case of real scalar fields, and in the appendix of [22], for complex ones, it was shown that for an appropriate superposition, a stress-energy-momentum tensor of the form (2.5) with $\Lambda = 0$ may be spherically symmetric, even though the individual fields Φ_i have non-vanishing angular momentum. Here, we generalize this result further to include the self-interaction of the field. The procedure is as follows.

Each scalar field Φ_i has the form

$$\Phi_i(t, r, \theta, \varphi) = \phi_\ell(t, r) Y^{\ell m}(\theta, \varphi), \quad i = \ell + 1 + m, \quad (2.6)$$

where m varies over $-\ell, -\ell + 1, \dots, \ell$ (such that i varies from 1 to $N = 2\ell + 1$) and $Y^{\ell m}(\theta, \varphi)$ denote the standard spherical harmonics. Here, the parameter ℓ is kept fixed and the amplitudes $\phi_\ell(t, r)$ are equal to each other for all m . Using the addition theorem for the spherical harmonics [31], one can show that the resulting stress-energy-momentum tensor in Eq. (2.5) for the $N = 2\ell + 1$ fields is spherically symmetric.

Next, one considers a stationary state with harmonic time dependence for the scalar field

$$\phi_\ell(t, r) = e^{i\omega t} \chi_\ell(r), \quad (2.7)$$

where χ_ℓ is function of r and ω is a real constant. Once such procedure is carried out, the following non-trivial components of the stress-energy-momentum tensor are obtained:

$$T^t_t = \frac{c^4}{8\pi G} \frac{2\ell + 1}{8\pi} \left\{ a \left(\frac{d\chi_\ell}{dr} \right)^2 + \left[\frac{\ell(\ell + 1)}{R^2} + \mu^2 - \frac{2\ell + 1}{4\pi} \Lambda \chi_\ell^2 + \frac{1}{a} \omega^2 \right] \chi_\ell^2 \right\}, \quad (2.8)$$

$$T^r_r = \frac{c^4}{8\pi G} \frac{2\ell + 1}{8\pi} \left\{ -a \left(\frac{d\chi_\ell}{dr} \right)^2 + \left[\frac{\ell(\ell + 1)}{R^2} + \mu^2 - \frac{2\ell + 1}{4\pi} \Lambda \chi_\ell^2 - \frac{1}{a} \omega^2 \right] \chi_\ell^2 \right\}, \quad (2.9)$$

$$T^\theta_\theta = T^\varphi_\varphi = \frac{c^4}{8\pi G} \frac{2\ell + 1}{8\pi} \left\{ a \left(\frac{d\chi_\ell}{dr} \right)^2 + \left[\mu^2 - \frac{2\ell + 1}{4\pi} \Lambda \chi_\ell^2 - \frac{1}{a} \omega^2 \right] \chi_\ell^2 \right\}. \quad (2.10)$$

Notice how the procedure of adding individual stress-energy-momentum tensors maintains the spherical symmetry and yields a result that depends on the angular momentum number ℓ through the centrifugal-like terms $\ell(\ell+1)/R^2$. As expected and shown below, this dependency plays a nontrivial role in the solutions of Einstein's equations. The mixed components T^t_r , T^t_θ and T^t_φ vanish; indicating that there are no fluxes of matter in this case, which is compatible with the assumption of staticity of the metric.

Notice also that the stress-energy-momentum tensor (2.8–2.10) violates the null energy condition everywhere; for instance, the null vector field $k = a^{-1/2}c^{-1}\partial_t + a^{1/2}\partial_r$ gives

$$T_{\mu\nu}k^\mu k^\nu = -T^t_t + T^r_r = -\frac{c^4}{8\pi G} \frac{2\ell+1}{4\pi} \left[a \left(\frac{d\chi_\ell}{dr} \right)^2 + \frac{\omega^2}{a} \chi_\ell^2 \right], \quad (2.11)$$

which is negative unless the scalar field vanishes.

Now, one can compute the equation of motion for each individual field, *i. e.* the Klein-Gordon equation, using the fact that the divergence of the total stress-energy-momentum tensor is zero. Each amplitude obeys the identical equation:

$$\frac{d}{dr} \left[a R^2 \frac{d\chi_\ell}{dr} \right] + R^2 \left(\frac{\omega^2}{a} - \frac{\ell(\ell+1)}{R^2} - \mu^2 + \frac{2\ell+1}{2\pi} \Lambda \chi_\ell^2 \right) \chi_\ell = 0, \quad (2.12)$$

where we have used the fact that spherical harmonics are eigenfunctions of the Laplace-Beltrami operator

$$\Delta_{S^2} Y^{\ell m} = \left(\frac{\partial^2}{\partial \theta^2} + \cot \theta \frac{\partial}{\partial \theta} + \frac{1}{\sin^2 \theta} \frac{\partial^2}{\partial \varphi^2} \right) Y^{\ell m} = -\ell(\ell+1) Y^{\ell m}. \quad (2.13)$$

As an example of the construction of the ℓ -wormhole by the contribution of individual non-spherical scalar fields, in Fig. 2 we show the distribution of the density at the throat for the fields $(\phi_1 Y^{1-1}, \phi_1 Y^{10}, \phi_1 Y^{11})$. The values are given by Eq. (2.5) for the $T^t_t \propto \rho$ component. This is the case for $\ell = 1$ wormhole, so that there are three values for m . The first sphere represents the sum of the $m = -1$ and $m = 1$ contributions, the second one represents the $m = 0$ field, and the combination is given in such a way that the total density (the third sphere) is spherically symmetric.

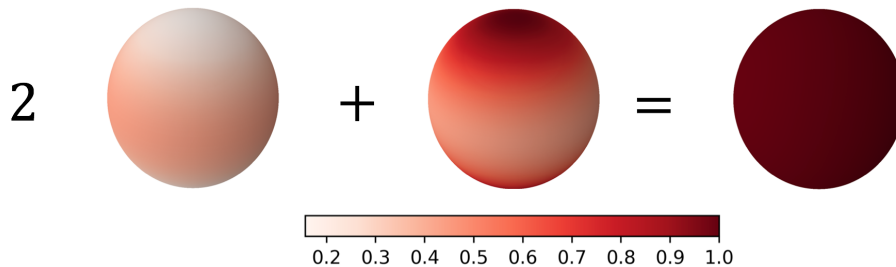


FIG. 2: Normalized density at the throat for a $\ell = 1$ wormhole. The first sphere represents the $m = \pm 1$ contribution while the center sphere corresponds to the $m = 0$ contribution.

III. STATIONARY WORMHOLE EQUATIONS

In order to obtain the remaining field equations, it is helpful to notice that with the stress-energy-momentum tensor components given by Eqs. (2.8, 2.9, 2.10) the following equation is satisfied

$$\frac{T^t_t - T^r_r}{2} - T^\theta_\theta = -\frac{c^4}{8\pi G} \frac{2\ell+1}{8\pi} \left(\mu^2 - \frac{2\ell+1}{4\pi} \Lambda \chi_\ell^2 - \frac{2}{a} \omega^2 \right) \chi_\ell^2. \quad (3.1)$$

On the other hand, from the line element Eq. (2.1), we obtain the Bianchi-Einstein tensor, G^μ_ν , and the same linear combination of the components gives:

$$\frac{G^t_t - G^r_r}{2} - G^\theta_\theta = -\frac{1}{2R^2} \frac{d}{dr} \left[R^2 \frac{da}{dr} \right]. \quad (3.2)$$

Thus, with the aid of Einstein's equations:

$$G^\mu{}_\nu = \frac{8\pi G}{c^4} T^\mu{}_\nu, \quad (3.3)$$

we obtain our next field equation:

$$\frac{1}{2R^2} \frac{d}{dr} \left[R^2 \frac{da}{dr} \right] = \frac{2\ell+1}{8\pi} \left(\mu^2 - \frac{2\ell+1}{4\pi} \Lambda \chi_\ell^2 - \frac{2}{a} \omega^2 \right) \chi_\ell^2. \quad (3.4)$$

Notice that when a static, massless scalar field (regular or exotic) without interaction is considered, then a particular solution is obtained in which the metric function a is constant.

A further field equation comes from the combination of the $G^t{}_t$ component plus the $G^r{}_r$ one, and the corresponding $T^\mu{}_\nu$ components:

$$\frac{dR^2}{dr} \frac{da}{dr} + a \frac{d^2 R^2}{dr^2} - 2 = \frac{2\ell+1}{4\pi} \left[R^2 \left(\mu^2 - \frac{2\ell+1}{4\pi} \Lambda \chi_\ell^2 \right) + \ell(\ell+1) \right] \chi_\ell^2. \quad (3.5)$$

As mentioned above, for the first independent field equation, we consider the Klein-Gordon equation, Eq. (2.12). In this way we obtain a system of equations in which each function $\chi_\ell(r)$, $a(r)$ and $R^2(r)$ appears as the only second derivative:

$$\chi_\ell'' = - \left(\frac{R^{2'}}{R^2} + \frac{a'}{a} \right) \chi_\ell' + \frac{1}{a} \left[\mu^2 - \frac{\omega^2}{a} + \frac{\ell(\ell+1)}{R^2} - \frac{2\ell+1}{2\pi} \Lambda \chi_\ell^2 \right] \chi_\ell, \quad (3.6)$$

$$a'' = - \frac{R^{2'}}{R^2} a' + \frac{2\ell+1}{4\pi} \left(\mu^2 - \frac{2}{a} \omega^2 - \frac{2\ell+1}{4\pi} \Lambda \chi_\ell^2 \right) \chi_\ell^2, \quad (3.7)$$

$$R^{2''} = \frac{1}{a} \left\{ -a' R^{2'} + 2 + \frac{2\ell+1}{4\pi} \left[\left(\mu^2 - \frac{2\ell+1}{4\pi} \Lambda \chi_\ell^2 \right) R^2 + \ell(\ell+1) \right] \chi_\ell^2 \right\}, \quad (3.8)$$

where a prime denotes derivative with respect to r . The remaining field equation is the rr -component of Eq. (3.3) which yields

$$\frac{R^{2'}}{2R^2} \left(a' + \frac{aR^{2'}}{2R^2} \right) - \frac{1}{R^2} = \frac{2\ell+1}{8\pi} \left[-a \chi_\ell^{2'} + \left(\mu^2 - \frac{2\ell+1}{4\pi} \Lambda \chi_\ell^2 - \frac{\omega^2}{a} + \frac{\ell(\ell+1)}{R^2} \right) \chi_\ell^2 \right], \quad (3.9)$$

which can be interpreted as a constraint since it only involves zeroth and first-order derivatives of the fields. Provided the second-order field equations (3.6, 3.7, 3.8) are satisfied, the twice contracted Bianchi identity $\nabla_\mu G^\mu{}_\nu = 0$ and $\nabla_\mu T^\mu{}_\nu = 0$ imply that

$$\frac{d}{dr} \left[aR^4 \left(G^r{}_r - \frac{8\pi G}{c^4} T^r{}_r \right) \right] = 0, \quad (3.10)$$

such that it is sufficient to solve Eq. (3.9) at one point (the throat, say).

A particular simple solution arises when a static, spherical, massless scalar field (regular or exotic) without interaction is considered. In this case, the parameters ω , μ , and Λ vanish and considering $\ell = 0$, the field equations (3.6–3.9) can be integrated explicitly [14, 15], see also [32]. The simplest (but not unique) solution is obtained assuming that the metric function a is constant. This yields the solution

$$a = 1, \quad R^2 = b^2 + r^2, \quad \chi_{\text{Ellis}}(r) = \sqrt{8\pi} \arctan \left(\frac{r}{b} \right), \quad (3.11)$$

which has the property that the metric functions a , R^2 and the gradient of χ_{Ellis} are reflection symmetric about the throat $r = 0$. In Fig. 3, we present the plot of Ellis' ghost field and the corresponding energy density. Although the scalar field itself does not decay to zero simultaneously at both asymptotic ends $r \rightarrow \pm\infty$, its gradient does. Since in the massless case the stress-energy-momentum tensor and equations of motion only depend on the gradient of the scalar field, the configuration is localized from a physical point of view. Furthermore, we observe that the density is negative everywhere. The curvature and Kretschmann scalars are given by $R_{s,\text{Ellis}} = -\frac{2b^2}{(r^2+b^2)^2}$ and $K_{\text{Ellis}} = R_{s,\text{Ellis}}^2$ (see Fig. 4), respectively, and like the density, they have a fixed sign.

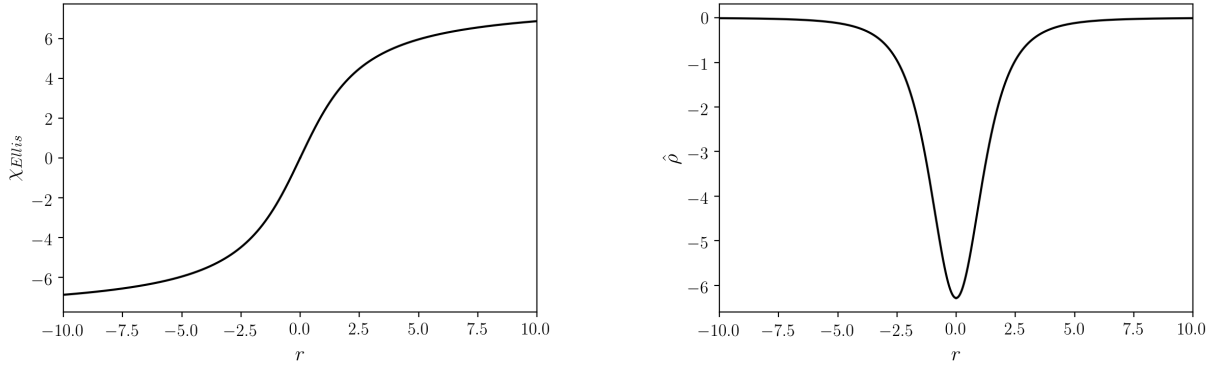


FIG. 3: Ghost field and the corresponding density for the original Ellis wormhole.

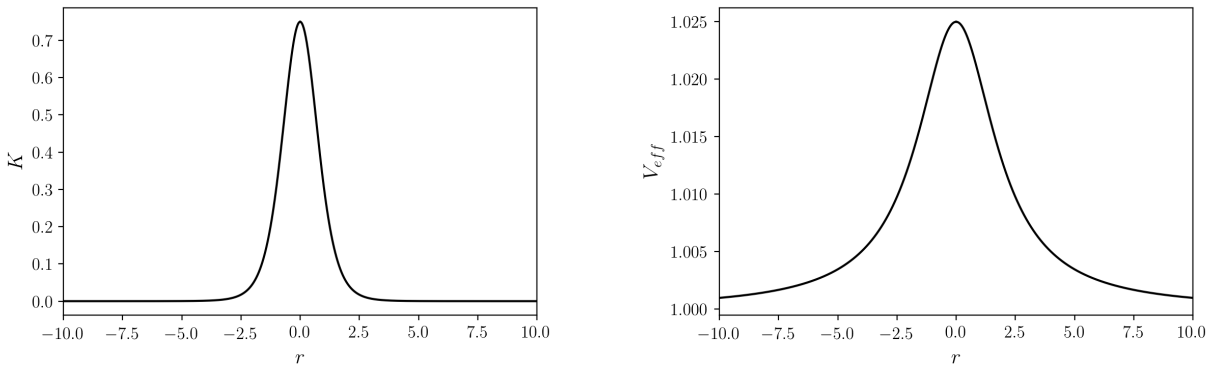


FIG. 4: Kretschmann scalar and effective potential, $V_{eff} = L^2/R^2 + \kappa$ for a massive particle propagating on the reflection-symmetric Ellis wormhole.

In the following, we consider much more general wormhole solutions in which the parameters ω , ℓ , μ and Λ do not necessarily vanish. These solutions are obtained by numerically integrating the field equations (3.6, 3.7, 3.8) and taking into account the constraint (3.9). For simplicity, in this article, we restrict ourselves to the reflection-symmetric case (although more general wormhole solutions which are asymmetric about the throat could also be considered). These solutions satisfy the following boundary conditions at the throat, $r = 0$:

$$\chi'_\ell(0) = 0, \quad (3.12)$$

$$a'(0) = 0, \quad (3.13)$$

$$R^{2'}(0) = 0. \quad (3.14)$$

Denoting by $b := R(0)$ the areal radius of the throat, the constraint (3.9) yields the following condition at $r = 0$:

$$\left[1 + \frac{(2\ell + 1)\ell(\ell + 1)}{8\pi} \chi_\ell(0)^2\right] b^{-2} = \frac{2\ell + 1}{8\pi} \left(\frac{\omega^2}{a(0)} - \mu^2 + \frac{2\ell + 1}{4\pi} \Lambda \chi_\ell(0)^2\right) \chi_\ell(0)^2, \quad (3.15)$$

which fixes the radius b of the throat and requires $a(0)$ and $\chi_\ell(0) \neq 0$ to be chosen such that

$$\frac{\omega^2}{a(0)} + \frac{2\ell + 1}{4\pi} \Lambda \chi_\ell(0)^2 > \mu^2. \quad (3.16)$$

Note that this inequality and Eq. (3.7) also imply that a has a local maximum at the throat. Next, Einstein's equation (3.8) together with the conditions (3.12, 3.13, 3.14), implies the relation

$$\frac{1}{2} a(0) (R^2)''(0) = \frac{2\ell + 1}{8\pi} \left[b^2 \left(\mu^2 - \frac{2\ell + 1}{4\pi} \Lambda \chi_\ell(0)^2 \right) + \ell(\ell + 1) \right] \chi_\ell^2(0) + 1. \quad (3.17)$$

Using Eq. (3.15) this can be simplified considerably,

$$\frac{1}{2}a(0)(R^2)''(0) = \frac{2\ell + 1}{8\pi} \frac{b^2\omega^2}{a(0)} \chi_\ell(0)^2, \quad (3.18)$$

which shows that the throat is indeed a local minimum³ of R^2 . For $\ell = 0$ the Eqs. (3.15, 3.18) reduce to the corresponding equations in Ref. [23] (see their equation (18) and the unnumbered equation below it.) Due to Eq. (3.15), one has two free parameters at the throat, given by $\chi_\ell(0) \neq 0$ and $a(0)$, say. As can be checked, the field equations (3.6, 3.7, 3.8, 3.9) as well as the conditions (3.15, 3.18) are invariant with respect to the transformations

$$(\omega, t, r, a, R^2, \chi_\ell) \mapsto \left(\frac{\omega}{\sqrt{B}}, \sqrt{B}t, \frac{r}{\sqrt{B}}, \frac{a}{B}, R^2, \pm\chi_\ell \right), \quad (3.19)$$

with $B > 0$ a real parameter. Therefore, one can fix the value of $a(0)$ to one, say, and adjust the value of B such that $a(r) \rightarrow 1$ for $r \rightarrow \infty$. In this way, one is left with just one shooting parameter ($\chi_\ell(0) > 0$, say) at the throat $r = 0$.

At $r \rightarrow \pm\infty$, we require asymptotic flatness,

$$\chi_\ell(r) \rightarrow 0, \quad (3.20)$$

$$a(r) \rightarrow 1, \quad (3.21)$$

$$\frac{R(r)}{r} \rightarrow 1. \quad (3.22)$$

Under these assumptions, the field equation (3.6) for the scalar field reduces to

$$\chi_\ell''(r) \approx (\mu^2 - \omega^2)\chi_\ell(r), \quad (3.23)$$

which shows that⁴

$$\omega^2 < \mu^2 \quad (3.24)$$

is required to have the exponentially decaying solution $\chi_\ell(r) \approx e^{-\sqrt{\mu^2 - \omega^2}r}$. Approximating the (exponentially decaying) right-hand sides of Eqs. (3.4, 3.5) to zero, one obtains the following behavior of the metric coefficients in the asymptotic region:

$$a \approx e^{-\frac{c_0}{r+c_1}}, \quad R^2 \approx (r+c_1)^2 e^{\frac{c_0}{r+c_1}}, \quad r \rightarrow \infty, \quad (3.25)$$

for some constants c_0 and c_1 .

A. Qualitative analysis of the solutions

Before numerically constructing the wormhole solutions, we make a few general remarks regarding the restrictions on the parameters ω , μ and Λ and the initial condition $\chi_\ell(0)$ and regarding the qualitative properties of the solutions. We assume in the following that $(\chi_\ell(r), a(r), R^2(r))$ is a smooth solution of Eqs. (2.12, 3.4, 3.5) (or, equivalently, of Eqs. (3.6, 3.7, 3.8)) on the interval $[0, \infty)$ which satisfies $a > 0$, $R^2 > 0$, the boundary conditions (3.12, 3.13, 3.14) at $r = 0$ and (3.20, 3.21, 3.22) at $r \rightarrow \infty$, and is subject to the conditions (3.15, 3.18) at the throat. We had already observed that an exponentially decaying solution at infinity requires $\omega^2 \leq \mu^2$. Furthermore, at the throat, the inequality (3.16) needs to be satisfied. A first immediate consequence of this last inequality is that the parameters ω and Λ cannot be both zero. In fact, one has the following stronger result which shows that the self-interaction term is needed.

Theorem 1 *There are no reflection-symmetric solutions with the above properties if $\Lambda = 0$.*

³ For $\omega \neq 0$ the right-hand side of Eq. (3.18) is positive since χ_ℓ and χ_ℓ' cannot both vanish at $r = 0$; otherwise it would follow from Eq. (3.6) that χ_ℓ vanishes identically. For the special case $\omega = 0$ see the proof of Theorem 2 below.

⁴ The limiting value $\omega^2 = \mu^2$ is discussed in Ref. [23].

Proof. We prove the theorem by contradiction. If $\Lambda = 0$, the inequality (3.16) implies that

$$\mu^2 < \frac{\omega^2}{a(0)} \leq \frac{\mu^2}{a(0)}, \quad (3.26)$$

which requires $a(0) < 1$ and $\omega^2 > 0$. However, Eq. (3.7) with $\Lambda = 0$ implies that at any point $r = r_c$ where the derivative of a vanishes, the equality

$$a''(r_c) = \frac{2\ell + 1}{4\pi} \left(\mu^2 - \frac{2\omega^2}{a(r_c)} \right) \chi_\ell(r_c)^2 \quad (3.27)$$

holds. Since $\mu^2 - 2\omega^2/a(0) < 0$, a has a local maximum at the throat, as already remarked above, such that $a(r)$ decreases for $r > 0$ small enough. Since $a(r) \rightarrow 1$ as $r \rightarrow \infty$ there must be a point $r = r_c$ for which a ceases to decrease, corresponding to a (local) minimum of a . At this point, we must have $a(r_c) < a(0)$, $a'(r_c) = 0$ and $a''(r_c) \geq 0$. On the other hand, since

$$\mu^2 - \frac{2\omega^2}{a(r_c)} < \mu^2 - \frac{2\omega^2}{a(0)} < 0, \quad (3.28)$$

Eq. (3.27) implies $a''(r_c) < 0$, provided that $\chi_\ell(r_c) \neq 0$, which leads to a contradiction. If $\chi_\ell(r_c) = 0$, we do not obtain an immediate contradiction since in this case it follows that $a''(r_c) = 0$. However, in this case, we must have $\chi'_\ell(r_c) \neq 0$ since otherwise χ_ℓ (as a solution of the second-order equation (3.6)) would be identically zero. By differentiating Eq. (3.7) twice with respect to r and evaluating at $r = r_c$ one obtains $a'''(r_c) = 0$ and

$$a''''(r_c) = \frac{2\ell + 1}{2\pi} \left(\mu^2 - \frac{2\omega^2}{a(r_c)} \right) \chi'_\ell(r_c)^2 < 0, \quad (3.29)$$

which shows that $r = r_c$ is a local maximum of a and yields again a contradiction. This concludes the proof of the theorem. \square

The next result implies that there cannot be more than one throat.

Theorem 2 *Under the assumptions stated at the beginning of this subsection, the function $R^2(r)$ is strictly monotonously increasing and strictly convex on the interval $[0, \infty)$.*

Proof. By combining Eqs. (3.8,3.9) one obtains the simple equation

$$\frac{(R^2)''}{R^2} = \frac{1}{2} \left[\frac{(R^2)'}{R^2} \right]^2 + \frac{2\ell + 1}{4\pi} \left(\chi_\ell'^2 + \frac{\omega^2}{a^2} \chi_\ell^2 \right) \quad (3.30)$$

for R^2 , which shows that $(R^2)'' \geq 0$ and hence that R^2 is convex. We show further that the right-hand side of Eq. (3.30) cannot vanish at any point. This is clearly the case if $\omega \neq 0$ since χ_ℓ' and χ_ℓ cannot vanish at the same point (otherwise it would follow from Eq. (3.6) that χ_ℓ is identically zero). Next, we rule out the exceptional case in which $\omega = 0$ and there existed a point $r_0 \geq 0$ where $(R^2)'(r_0) = \chi_\ell'(r_0) = 0$. If this case occurred, successive differentiation of Eq. (3.30) would yield

$$(R^2)'''(r_0) = 0, \quad \frac{(R^2)''''(r_0)}{R^2(r_0)} = \frac{2\ell + 1}{2\pi} [\chi_\ell''(r_0)]^2. \quad (3.31)$$

Further, evaluating Eq. (3.9) at $r = r_0$ one would obtain

$$-\frac{1}{R^2(r_0)} = \frac{2\ell + 1}{8\pi} \left(\mu^2 - \frac{2\ell + 1}{4\pi} \Lambda \chi_\ell(r_0)^2 + \frac{\ell(\ell + 1)}{R^2(r_0)} \right) \chi_\ell(r_0)^2, \quad (3.32)$$

implying that $\chi_\ell(r_0) \neq 0$ and that the expression inside the parenthesis on the right-hand side must be negative. Eq. (3.6) would then imply that

$$a(r_0) \frac{\chi_\ell''(r_0)}{\chi_\ell(r_0)} < -\frac{2\ell + 1}{4\pi} \Lambda \chi_\ell(r_0)^2 < 0, \quad (3.33)$$

and hence $\chi_\ell''(r_0) \neq 0$ and $(R^2)''''(r_0) > 0$. It follows that any critical point of R^2 must be a strict minimum of R^2 . However, since R^2 is convex there can be only one such critical point which is the one at the throat. Therefore, it follows from Eq. (3.30) that $(R^2)''(r) > 0$ for all $r > 0$ and the theorem is proven. \square

$\omega = 0$	$\ell = 0$			$\ell = 1$			$\ell = 2$		
	$\chi_\ell(0)$	$R(0)$	$a(0)$	$\chi_\ell(0)$	$R(0)$	$a(0)$	$\chi_\ell(0)$	$R(0)$	$a(0)$
$\Lambda = 0.5$	6.26	1.07	1.40	3.94	1.72	7.43	3.08	2.71	20.21
$\Lambda = 0.7$	4.91	1.75	0.80	3.21	1.97	2.59	2.58	2.81	7.04
$\Lambda = 1.0$	3.90	2.79	0.58	2.48	2.70	1.03	2.08	3.14	2.51
$\Lambda = 4.0$	1.81	13.21	0.41	1.05	13.14	0.42	0.82	13.00	0.44

TABLE I: Central values of the field χ_ℓ and metric functions R and a for several values of $\Lambda = 0.5, 0.7, 1.0, 4.0$ and $\ell = 0, 1, 2$ with $\omega = 0$.

B. Numerical shooting algorithm

Next, we describe a shooting algorithm which allows us to find asymptotically flat wormhole solutions from a given set of initial conditions at the throat by numerically integrating the equations outwards. As discussed above, there is only one free parameter to start the shooting procedure. Such parameter is the value of the scalar field at the throat, $\chi_\ell(0)$.

We are looking for the desired solutions in the same spirit as the boson stars (see for instance [33]), in which the solutions are parametrized by the value of the scalar field at the center of the configuration so that for each solution a set of discrete values for the frequency is found to satisfy the asymptotic flatness conditions, each with different number of nodes for the scalar field profile. Qualitatively, the same happens with the ℓ -wormhole solutions discussed here. All the solutions reported in this article are those corresponding to the ground state, in which the scalar field χ_ℓ has no nodes.

So for given values of $a(0)$, Λ , ℓ , ω , only one particular value of $\chi_\ell(0)$ picks the $\chi_\ell \rightarrow 0$ solution at infinity. We can see this in the approximation of the Klein-Gordon equation for large r . If we assume that $a(r)$ tends to unity and $R(r)$ to the coordinate r fast enough, then Eq. (3.23) is satisfied, which is consistent with exponential decay of χ_ℓ for large r as long as $\mu^2 - \omega^2 > 0$. In a similar way we see that if χ_ℓ is exponentially decaying at both infinities then, from (3.7) we obtain $\frac{d^2 a}{dr^2} + \frac{2}{r} \frac{da}{dr} \approx 0$, which has solutions:

$$a \approx B + \frac{A}{r}, \quad (3.34)$$

where A and B are constants. This is a particular simplification over Eq. (3.25) that is useful in the numerical procedure. In particular B will enter as a normalization factor, since we will ask for $B = 1$, as required by the asymptotic condition (3.21).

As mentioned previously, $\chi_\ell(0)$ is used as the shooting parameter so the requirements needed to find a solution are those described in the previous paragraphs. Using the LSODA FORTRAN solver for initial value problems of ordinary differential equations, we perform the integration of the system (3.6–3.8) starting at the value $r = 0$ using steps of $\Delta r = 1 \times 10^{-6}$ until a final value is reached. This finite value of the asymptotic boundary needs to be sufficiently large for the functions to reach their asymptotic behavior. Once the desired behavior of χ_ℓ is obtained up to a precision of order Δr , the asymptotic values of R and a are adjusted by means of the transformation (3.19) which leaves the system of equations invariant, where the parameter B is chosen equal to the corresponding coefficient in Eq. (3.34).

Examples are shown in Tables I and II. Their physical implications are shown in section IV. The 0-wormhole recovers the wormhole studied by Dzhunushaliev *et al.* in [23] for complex, massive and self-interacting ghost scalar fields. Our results match those of them as can be seen in the $\Lambda = 4.0$ row in Table I when the following change of variables is performed:

$$r \mapsto \int_0^r \frac{dr}{\sqrt{a(r)}}, \quad \Lambda \mapsto \frac{\Lambda}{4}, \quad \chi_\ell \mapsto \sqrt{\frac{8\pi}{2\ell+1}} \chi_\ell, \quad (3.35)$$

which takes into account the differences in the definitions, nondimensionalization and the coordinate election. These authors also studied the case for a real scalar field in a previous work [24], which in fact corresponds to the $\omega = 0$ results in this paper.

$\Lambda = 0.7$	$\ell = 0$			$\ell = 1$			$\ell = 2$				
	$\chi_\ell(0)$	$R(0)$	$a(0)$	$\chi_\ell(0)$	$R(0)$	$a(0)$	$\chi_\ell(0)$	$R(0)$	$a(0)$		
$\omega = 0.1$	4.88	1.77	0.83	$\omega = 0.3$	3.18	2.01	2.60	$\omega = 0.8$	2.56	2.85	7.03
$\omega = 0.2$	4.64	2.01	1.07	$\omega = 0.5$	2.95	2.34	2.82	$\omega = 1.0$	2.36	3.28	7.13
$\omega = 0.3$	4.06	3.01	2.25	$\omega = 0.8$	2.45	3.67	4.49	$\omega = 1.6$	1.94	5.01	9.77

TABLE II: Central values of the field χ_ℓ and metric functions R and a for several values of ω and $\ell = 0, 1, 2$ with $\Lambda = 0.7$.

C. Energy density, mass and curvature scalars

In order to help interpreting the solutions presented in the next section, we discuss several scalar quantities, like the energy density ρ of the ghost field measured by static observers, the Misner-Sharp mass function and the scalars related with the curvature of the spacetime, such as the Ricci scalar R_s and the Kretschmann scalar K . These quantities will turn out to be helpful for understanding the features of the ghost field and its action on the geometry.

Explicitly, the function ρ , associated with the density of the ghost field, is given by

$$\rho = -\frac{T^t_t}{c^2} = \left(\frac{c^2}{8\pi G}\right) \hat{\rho}, \quad (3.36)$$

where $\hat{\rho}$ is defined by

$$\hat{\rho} = -(2\ell + 1) \left[a \chi_\ell'^2 + \left(\frac{\ell(\ell + 1)}{R^2} + \mu^2 - \frac{2\ell + 1}{4\pi} \Lambda \chi_\ell^2 + \frac{\omega^2}{a} \right) \chi_\ell^2 \right]. \quad (3.37)$$

A striking feature of the wormhole solutions is that despite the presence of the exotic matter which violates the null energy condition everywhere, the density may still be *positive* at the throat,⁵ as will be shown in the numerical examples discussed in the next section. In fact, using Eq. (3.9) one can obtain the following simple expression for $\hat{\rho}$ at the throat:

$$\hat{\rho}(0) = \frac{8\pi}{b^2} - 2(2\ell + 1) \frac{\omega^2}{a(0)} \chi_\ell(0)^2, \quad (3.38)$$

which shows explicitly that for those solutions with $\omega = 0$ the energy density is indeed positive near the throat. The plots in the next section show that this behavior also holds for other solutions with small enough values of ω^2 .

The total (ADM) mass of the wormhole configurations can be computed from the asymptotic limit $M_\infty = \lim_{r \rightarrow \infty} M(r)$ of the Misner-Sharp mass function [34] $M(r)$, defined by

$$\frac{2GM}{c^2} = R [1 - g^{\mu\nu} (\nabla_\mu R) (\nabla_\nu R)] = R (1 - aR'^2). \quad (3.39)$$

From Eqs. (3.25, 3.34) one obtains $GM_\infty/c^2 = c_0/2 = -A/2$. Alternatively, using Eqs. (3.8, 3.9) one also obtains $M' = 4\pi\rho R^2 R'$ which can be integrated to

$$M(r) = \frac{c^2}{2G} \left(b + \int_0^r \hat{\rho}(\bar{r}) R^2(\bar{r}) R'(\bar{r}) d\bar{r} \right), \quad (3.40)$$

with $b = R(0)$ the throat's areal radius. As long as $\hat{\rho}$ is positive near the throat, the mass function increases as one moves away from the throat. However, M decreases as soon as $\hat{\rho}$ becomes negative, so that solutions which have either sign of the total mass are possible. This is shown in Table III, where values of the total mass M_∞ for our wormhole were computed taking several values of ℓ and fixing the values of all other parameters.

⁵ Note that the violation of the null energy condition implies the violation of the weak energy condition, which means that there exists at least one observer which measures negative energy density. Our example shows that this observer does not necessarily need to be a static one.

$\omega = 0, \Lambda = 1$	$M_\infty (m_{\text{pl}}^2/m_\Phi)$
$\ell = 0$	0.677
$\ell = 1$	0.224
$\ell = 2$	-1.25
$\ell = 3$	-4.69

TABLE III: Total mass values for ℓ -wormholes with $\Lambda = 1$, $\omega = 0$ and $\ell = 0, 1, 2, 3$.

The Ricci scalar, $R_s = R^\mu{}_\mu$, associated with the geometry given by Eq. (2.1) has the form

$$R_s = -a'' - 2a \frac{R^{2''}}{R^2} + a \left(\frac{R^{2'}}{R^2} \right)^2 + \frac{2}{R^2} (1 - a' R^{2'}). \quad (3.41)$$

A further commonly used curvature measure is the Kretschmann scalar, defined by $K = R^{\mu\nu\sigma\tau} R_{\mu\nu\sigma\tau}$. For the metric under consideration, Eq. (2.1), the Kretschmann scalar has the following explicit form:

$$K = a'' + 2 \left(\frac{a R^{2''}}{R^2} \right)^2 + 2a \frac{R^{2''} R^{2'}}{R^4} \left(a' - \frac{a R^{2'}}{R^2} \right) + \frac{4}{R^4} + \left[\frac{3}{4} \left(\frac{a R^{2'}}{R^2} \right)^2 - \frac{a^{2'} R^{2'}}{2 R^2} + a'^2 - 2 \frac{a}{R^2} \right] \left(\frac{R^{2'}}{R^2} \right)^2. \quad (3.42)$$

All these quantities will turn out to be helpful when understanding the role played by the several parameters of the solution in the geometry and in the dynamics of the bodies moving on it.

From Einstein's equations, Eq. (3.3), we have that $R_s = -\frac{8\pi G}{c^4} T$ with T the trace of the stress-energy-momentum tensor. Numerical experiments show that the behavior of the stress-energy-momentum tensor components in the throat region are similar to each other, and thus $R_s \approx \frac{8\pi G}{c^2} \rho$, as seen in the actual solutions. That is, the Ricci scalar goes as the density, irrespective of its character, exotic or usual matter. We will discuss this fact in more detail in the explicit cases that we present below.

IV. NUMERICAL WORMHOLE SOLUTIONS

Following the procedure described above, we are able to obtain several solutions to the Einstein-Klein-Gordon system, given the four parameters, namely μ, ω, Λ , and ℓ . We will present the solutions first for trivial values of the angular momentum parameter, $\ell = 0$, and vary the self-interaction parameter Λ , while keeping the oscillation frequency ω fixed and then we explore the properties of the solution for some values of ω maintaining Λ fixed, as was done in [23, 24]. Next, we repeat the study for different values of ℓ . In all our solutions presented in this work, we keep the mass of the scalar field μ fixed. These experiment allow us to have a better understanding on the role that each parameter plays in determining the geometry of the solutions.

All the solutions presented are asymptotically flat, and are generated by looking for a solution of the ghost scalar field, once the parameters ℓ, Λ and ω are chosen. We fix the value of mass parameter μ to one, and the distance scale of the solution is given by the dimensionless parameter $\hat{r} = \mu r$. Also, from Eq. (3.15) we see that the size of the wormhole throat $R(0)$ is given by

$$R(0) = \left(\frac{\ell(\ell+1) + \frac{8\pi}{(2\ell+1)\chi_\ell^2(0)}}{\frac{2\ell+1}{4\pi}\Lambda\chi_\ell^2(0) + \frac{\omega^2}{a(0)} - \mu^2} \right)^{1/2}. \quad (4.1)$$

In Fig. 5, we present this localized solution, for the case $\ell = 0, \omega = 0$, for several values of Λ . All the other solutions with $\ell > 0$ are localized as well. Notice how the amplitude of the pulse decreases as the value of the self-interaction parameter Λ increases.

In our experiments, we see that the ghost density, in order to form a wormhole, is distributed in such a way that it has a positive value in the region of the throat, and then it starts to have larger concentrations of negative ghost density on both sides of the throat, as shown in Fig. 6. From the geometric perspective, as suggested above, the profile of the Ricci scalar follows the density one and has a convex region at the throat, surrounded by concave zones, see Fig. 8.

Also we will show that, in general, as can be seen in Fig. 6, the action of the self-interaction parameter, Λ , smooths out this behavior of the exotic density and spacetime interaction. Indeed, the scalar field, at least the massive ghost

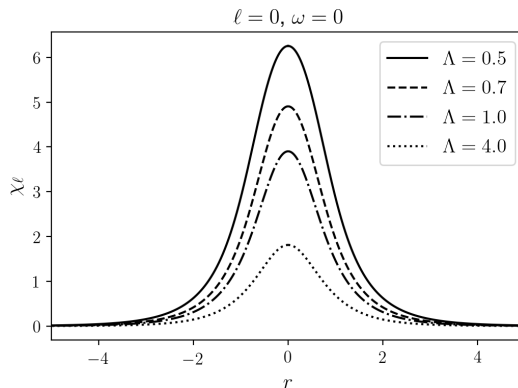


FIG. 5: Solitonic profile for the 0-wormhole, for $\Lambda \in [0.5, 4.0]$, and $\omega = 0$.

field, possess a radial pressure that creates the throat and then the spacetime strongly reacts generating regions of negative density; it is the role of the self-interaction term to smooth down such reaction and allows to keep the wormhole throat open with smaller amount of ghost density. Conversely, as the self-interaction parameter Λ becomes smaller, the metric coefficient a , the curvature scalars and density at the throat become more and more localized, an observation which is compatible with the result in Theorem 1 where we have shown that the solutions cease to exist for $\Lambda = 0$.

A. 0-wormhole

We start our discussion for the case with vanishing angular momentum, *i. e.* $\ell = 0$. Setting also ω equal to zero for the moment, we start by sweeping a range of values for the self-interaction parameter, Λ . The corresponding results for the scalar field and the density profile are shown in Figs. 5 and 6, respectively. As mentioned above, the ghost density has regions of positive magnitude near the throat, and regions with negative density which tend to zero from below in the asymptotic region.

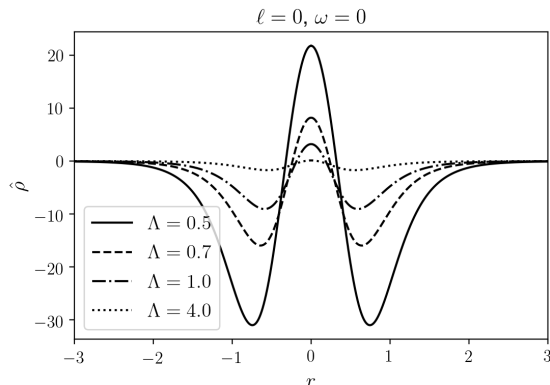


FIG. 6: Density profile for the 0-wormhole, for $\Lambda \in [0.5, 4.0]$ and $\omega = 0$.

The corresponding metric coefficients, $a(r)$ and $R(r)$ are shown in Fig. 7. Notice how the metric coefficient $a(r)$ shows concave regions which will determine a similar behavior in the effective potential of the spacetime, which in turn will imply the existence of particles moving on bound trajectories. Again, the effect of the self-interaction parameter is to smooth out the concavity of the metric functions.

Regarding the curvature scalars, as expected, the Ricci scalar R_s has a behavior which follows the one of the density, with regions of positive values and then valleys with negative values of the curvature as we can see in Fig. 8. The Kretschmann scalar, however, is very different and shows two peaks of positive values and they decrease as the self-interaction parameter grows, and the central one is negative in the region of the throat, surrounded by bumps.

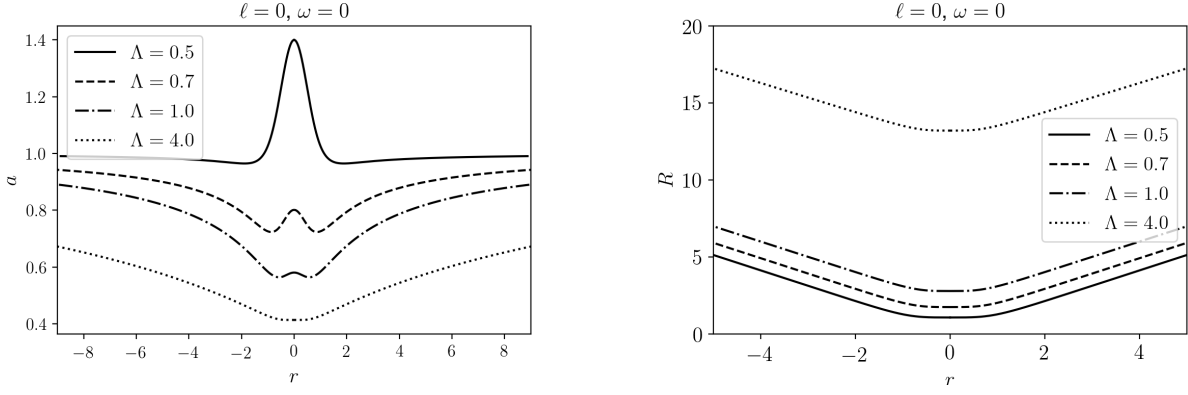


FIG. 7: Metric coefficients for $\Lambda \in [0.5, 4.0]$ and $\omega = 0$.

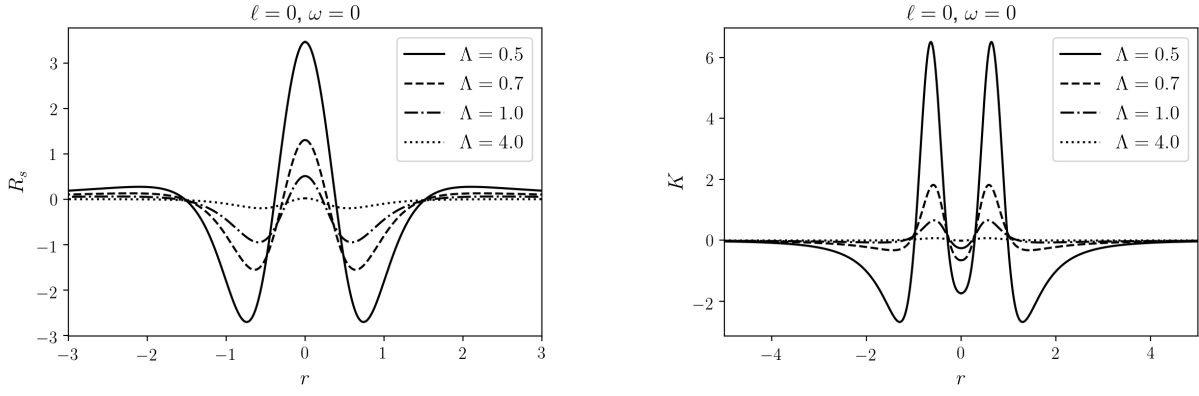


FIG. 8: Ricci and Kretschmann scalars for $\Lambda \in [0.5, 4.0]$ and $\omega = 0$.

The next step is to increase the parameter ω keeping $\ell = 0$ and the self-interaction parameter $\Lambda = 0.7$ fixed. We show in Fig. 9 the corresponding density and Kretschmann scalar for three non-zero values, $\omega = 0.1, 0.3, 0.5$, of the frequency. Notice the difference between the behavior of the Kretschmann scalar, in which a larger value of ω gives the effect of increasing the central value, acting in the same way as the parameter Λ discussed above.

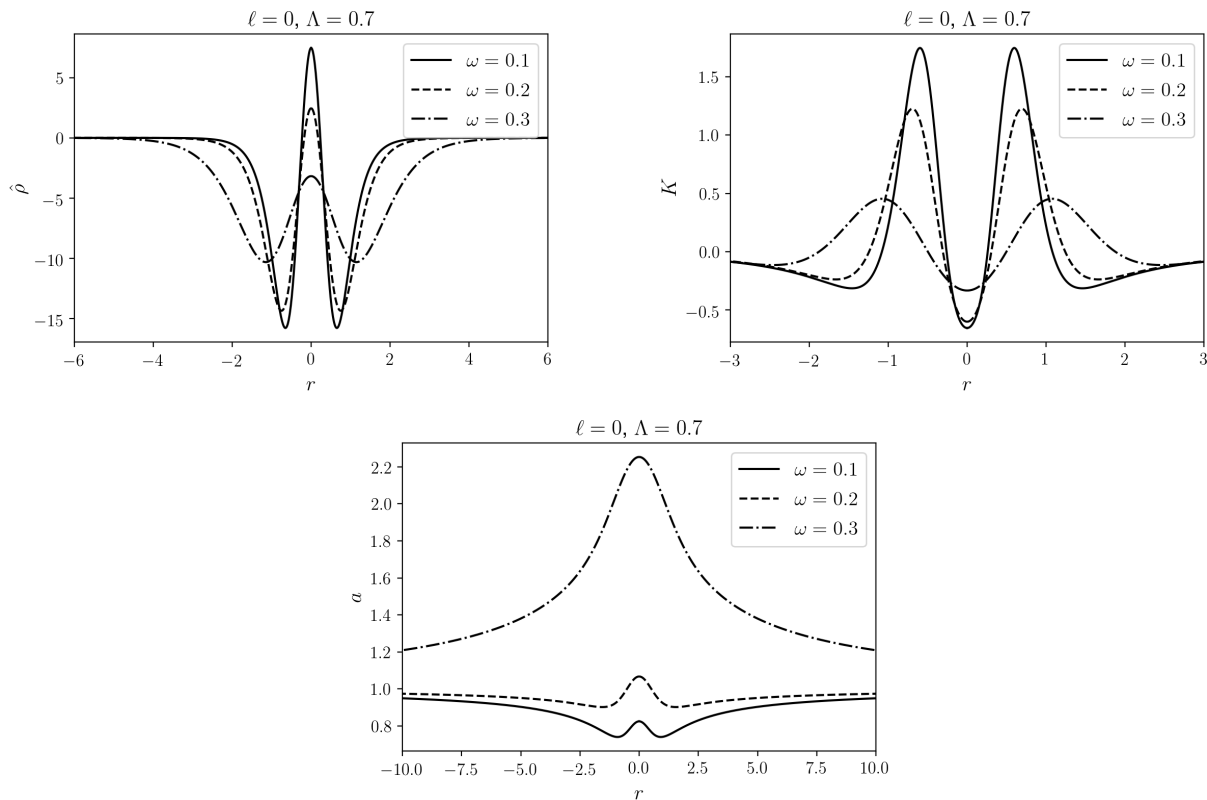


FIG. 9: Density profile, curvature scalar and metric function a for the 0-wormhole, $\Lambda = 0.7$ and $\omega = 0.1, 0.2, 0.3$.

B. ℓ -wormhole

In this section we present the behavior of the ℓ parameter and the effect on the metric functions and the curvature scalars. For the latest we can see in Fig. 10 that an increment on the ℓ parameter increases the central peak for the Ricci scalar and decreases the central bump for the Kretschmann scalar. The case for $a(r)$ is quite different: while for $\ell = 1$ the two minima are still present, for larger values of the ℓ parameter the central peak is increased and the minima disappear. The presence of a minimum (or two in this case) also corresponds to positive total masses as can be verified in Table III and Fig. 11, consequently, its absence corresponds to negative masses. This is a general property of all solutions given the asymptotic behavior of a (see Eq. 3.34).

On the other hand, as is shown in Fig. 12, the increment of the ω parameter plays a role quite similar to the one made by the ℓ parameter: an increase on the former elevates the central peak on the metric function $a(r)$.

Moreover, as can be seen from a comparison of Figs. 7 and 10, the effect of the Λ parameter on the metric coefficient a is opposite to the one generated by the ℓ parameter on that metric coefficient. Indeed, for small values of Λ , the metric coefficient a has a global maximum at the throat, while for large values of this Λ , the metric coefficient a only has a local maximum. Thus, for small values of Λ , the ℓ parameter is not able to change the qualitative behavior of the metric coefficient, while for larger values of Λ , the appearance of the local maximum is recovered or enhanced with the parameter ℓ . This fact will have consequences on the effective potential and the geodesic motion of particles, as discussed below.

V. EMBEDDING DIAGRAMS AND GEODESIC MOTION

In order to gain a better understanding of the configurations described by the scalar field and the geometry in the vicinity of the throat, in this section we discuss the embedding procedure and geodesic motion. Because the metric (2.1) is static and spherically symmetric, it is sufficient to analyze the induced geometry on a $t = \text{constant}$ and $\theta = \pi/2$ slice, described by the two-metric

$$d\Sigma^2 = a^{-1}dr^2 + R^2d\phi^2 . \quad (5.1)$$

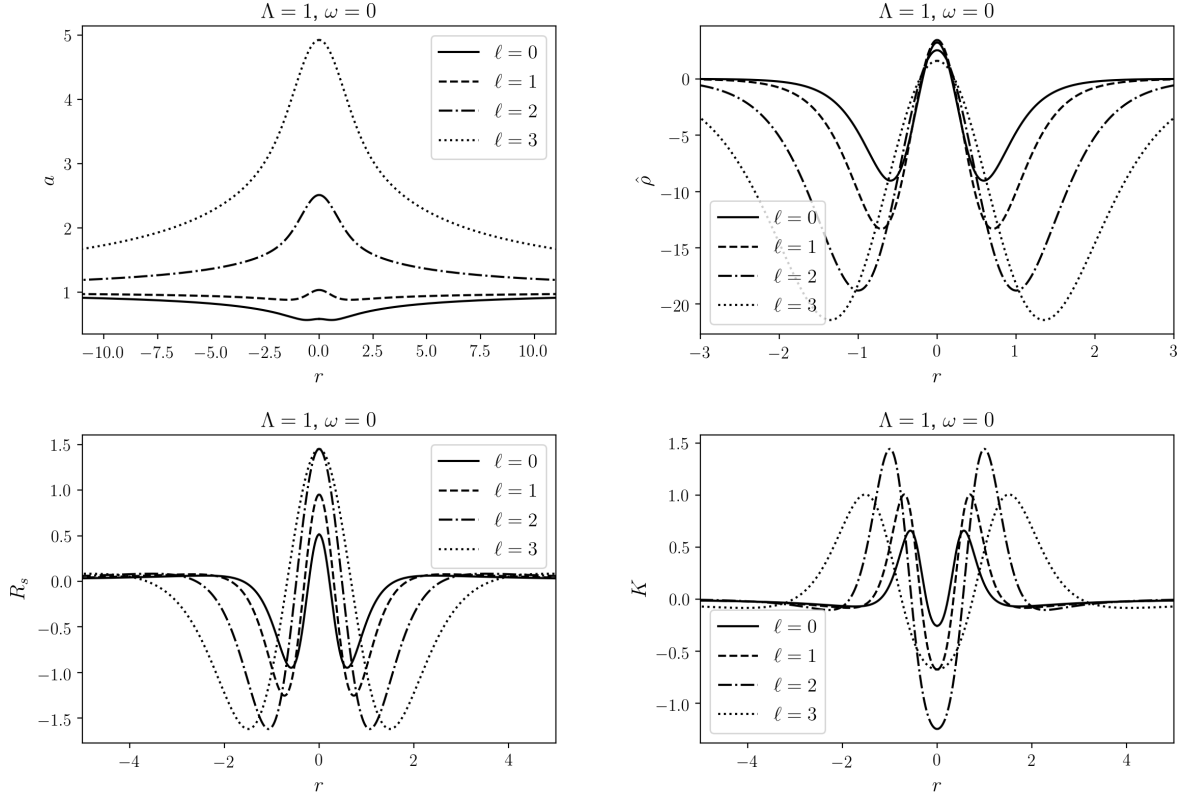


FIG. 10: Metric function $a(r)$, density profile $\hat{\rho}$ and R_s , K scalars for $\ell \geq 0$, $\Lambda = 1.0$ and $\omega = 0$.

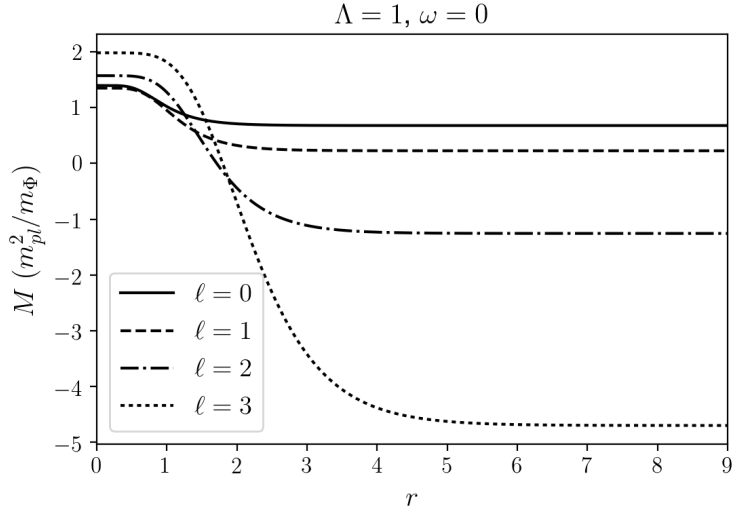


FIG. 11: Mass function $M(r)$ for the parameters $\ell \geq 0$, $\Lambda = 1$ and $\omega = 0$.

In order to visualize this geometry as a two-dimensional surface embedded in three-dimensional flat space we shall employ cylindrical coordinates (ρ, φ, z) . The metric for a flat space in these coordinates is

$$dS^2 = d\rho^2 + \rho^2 d\varphi^2 + dz^2. \quad (5.2)$$

We seek for the functions $\rho(r)$ and $z(r)$, specifying a surface with the same geometry as the one described by the metric (5.1).

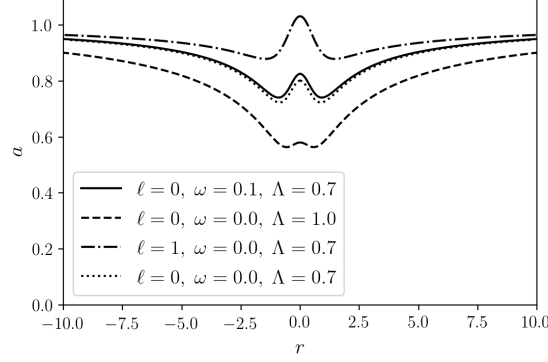


FIG. 12: Metric function a for different values of the parameters ℓ , ω and Λ .

The line element for the embedding surface will be

$$d\Sigma^2 = \left[\left(\frac{dz}{dr} \right)^2 + \left(\frac{d\rho}{dr} \right)^2 \right] dr^2 + \rho^2 d\varphi^2, \quad (5.3)$$

if the following conditions are satisfied:

$$\rho = R, \quad (5.4)$$

and

$$\left(\frac{dz}{dr} \right)^2 + \left(\frac{d\rho}{dr} \right)^2 = \frac{1}{a}. \quad (5.5)$$

Using the expression (5.4) to calculate $\frac{d\rho}{dr}$, Eq. (5.5) gives the following differential equation for $z(r)$:

$$\frac{dz}{dr} = \left[\frac{1}{a} - \frac{1}{4} \frac{(R^{2'})^2}{R^2} \right]^{1/2}. \quad (5.6)$$

Integrating this equation gives the function $z = z(r)$; in order to plot it in an Euclidean space, we need to find r as a function of ρ . However, it is not possible to express this function $r = r(\rho)$ in closed form because R was found numerically. Nevertheless, one can obtain $r = r(\rho)$ numerically from (5.4) and finally get $z = z(\rho)$.

In Fig. 13 we show the visualization of this embedding. It is seen that as ℓ increases from 0 to 2, the profile of the embedding representing the wormhole's geometry becomes more and more curved (which is analogous to the increase of $|R_s|$ and $|K|$ shown in Fig. 10), with a slight decrease in the throat's radius.

A. Geodesic motion

In order to describe the motion of the particles in the spacetimes described above, we start from the Lagrangian for the metric (2.1),

$$\mathcal{L} = g_{\mu\nu} u^\mu u^\nu + \kappa c^2 = -ac^2 (u^0)^2 + a^{-1} (u^r)^2 + R^2 [(u^\theta)^2 + \sin^2 \theta (u^\varphi)^2] + \kappa c^2, \quad (5.7)$$

where $u^\mu = \dot{x}^\mu$ is the four velocity and the parameter κ assumes the values 1 or 0, depending on whether the particle is massive or massless. The line element is spherically symmetric and static, so that the energy, $E = -\frac{\partial \mathcal{L}}{\partial u^0}$, the azimuthal momentum, $L_\varphi = \frac{\partial \mathcal{L}}{\partial u^\varphi}$, and the total angular momentum, $L^2 = \left(\frac{\partial \mathcal{L}}{\partial u^\theta} \right)^2 + \frac{L_\varphi^2}{\sin^2 \theta}$, are conserved quantities. Explicitly, they have the form:

$$E = -\frac{\partial \mathcal{L}}{\partial u^0} = ac^2 u^0, \quad (5.8)$$

$$L_\varphi = \frac{\partial \mathcal{L}}{\partial u^\varphi} = R^2 \sin^2 \theta u^\varphi. \quad (5.9)$$

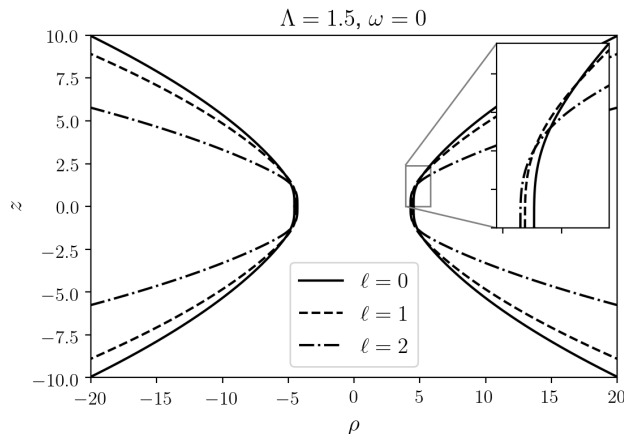


FIG. 13: Embedding of the different ℓ -wormholes, for $\Lambda = 1.5, \omega = 0$. The complete embedding diagram is obtained by rotating this figure about the z axis. In the enlarged picture we underline the change of the value of the throat radius for the given values of ℓ .

Since we are only interested in the motion of a single particle (as opposed to a swarm of particles) we can choose the angles such that the orbital plane coincides with the equatorial plane $\theta = \pi/2$, in which case $L_\varphi = L$. In this way, we can express the components of the four-velocity in terms of the conserved quantities L and E , and the normalization condition $g_{\mu\nu} u^\mu u^\nu = -\kappa c^2$ yields the radial equation of motion:

$$(u^r)^2 + V_{\text{eff}} = \frac{E^2}{c^2}, \quad (5.10)$$

with the effective potential

$$V_{\text{eff}} = \frac{a L^2}{R^2} + a \kappa c^2. \quad (5.11)$$

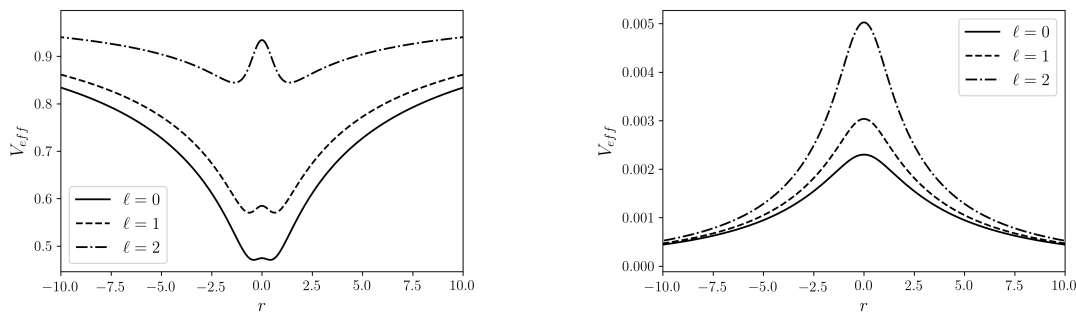


FIG. 14: Effective potential for time-like (left panel) and null geodesics (right panel) for $L = \sqrt{\frac{1}{10}}$.

In Fig. 14 we plot V_{eff} for the parameter choices $L = \sqrt{\frac{1}{10}}$, $\omega = 0$ and $\Lambda = 1.5$ for time-like and a null geodesics. As expected, the term involving L generates an angular momentum barrier, corresponding to a local maximum of the effective potential located at the throat $r = 0$. (Recall from Section III that $a(r)$ has a local maximum while $R^2(r)$ has a local minimum at $r = 0$.) This maximum corresponds to an unstable equilibrium point giving rise to circular unstable particle orbits. For the $\ell = 0$ case, and for this value of L and with $\kappa = 1$, the effective potential also has a minimum at $r \approx \pm 1.34$, which means that bound orbits also exist for this value of L .

In Fig. 15 we plot different geodesics for massive particle with $L = \sqrt{1/10}$ and $\Lambda = 1.5$ in the $\ell = 0, 1, 2$ wormholes. Here we picked the same initial conditions in terms of the initial radial velocity $u^r(0) = 0$ and initial position $r(0) = 0.65$, $\varphi(0) = \pi$ ending up with particles with different energies and qualitatively different motion. As stated

above, one can assume without loss of generality that the motion is confined to the equatorial plane $\theta = \frac{\pi}{2}$, so that it can be plotted in the embedding surface. As can be noticed from the plots, the motion is quite interesting and can be understood based on the behavior of the effective potential and the energy level of the test particle.

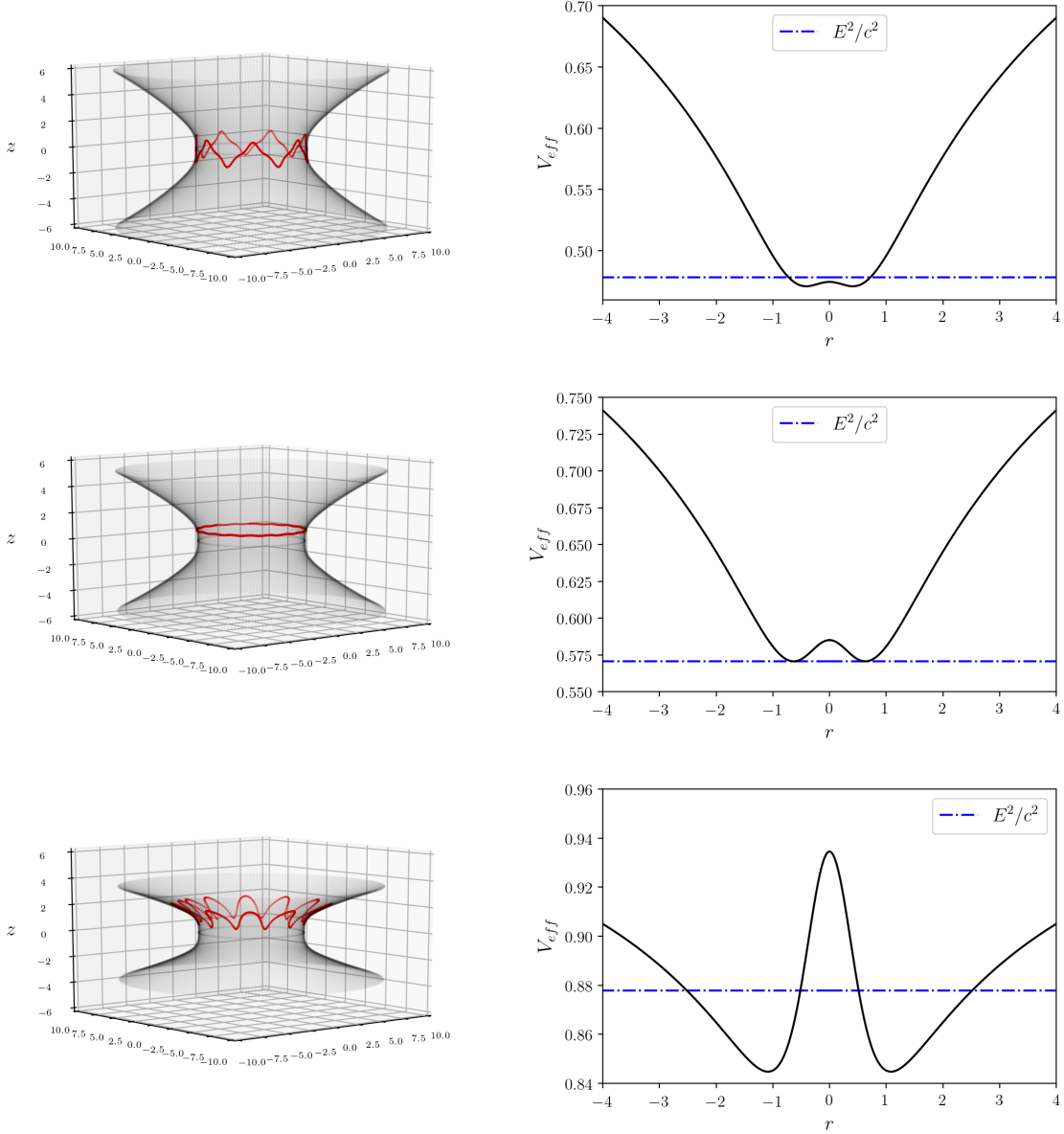
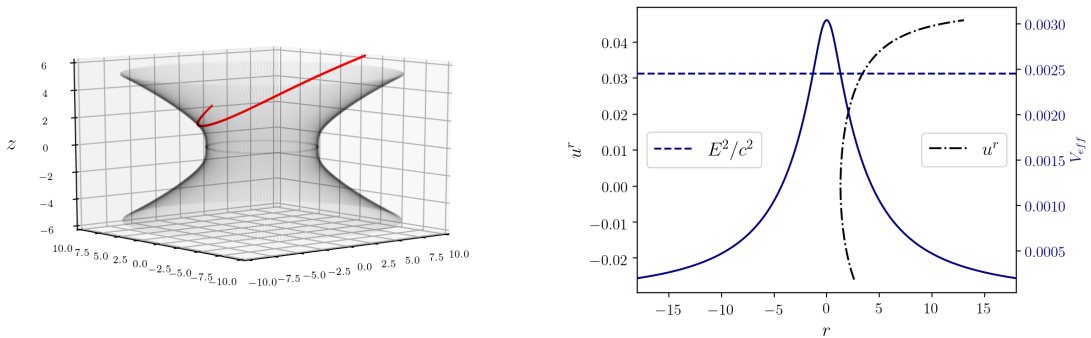
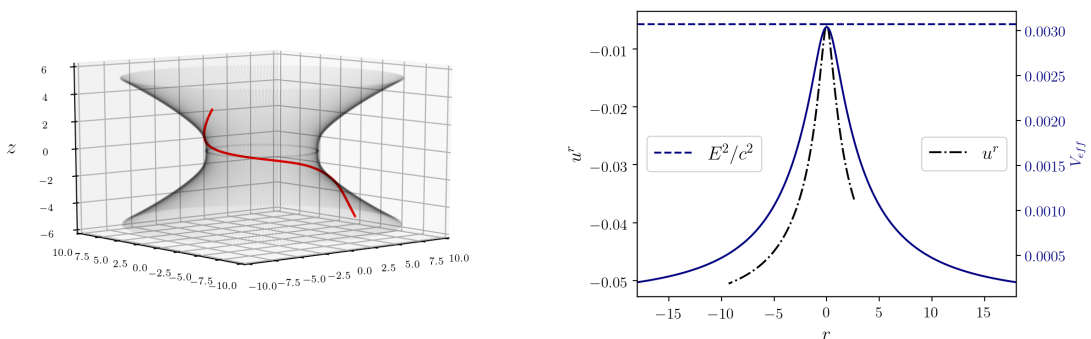


FIG. 15: Different $\ell = 0$ (top), $\ell = 1$ (middle) and $\ell = 2$ (bottom) geodesics for $\kappa = 1$, $\omega = 0$, $\Lambda = 1.5$, $L = \sqrt{1/10}$. On the left we plot the motion of the particle in the embedding surface of the wormhole and on the right the value of E and V_{eff} .

In order to further clarify the behavior of the geodesics, in Fig. 16 we plot the trajectory in the embedding diagram and the radial velocity u^r for two different null geodesics with angular momentum $L = \sqrt{1/10}$ propagating in the $\ell = 1$ wormhole. In the first case, shown in Fig. 16a, the particle does not have sufficient energy to traverse the throat so it starts approaching the throat with a decrement of the velocity, reaches a zero radial velocity and resumes its motion going away from the throat. On the other hand, the second example in Fig. 16b shows that, for a particle that has enough energy to pass through the throat, the absolute value of its velocity decreases as it moves towards the throat (from right to left) until it traverses the throat, after which the absolute value of the velocity increases again as the particle moves away from the throat on the other side of the wormhole.



(a) A particle having insufficient energy to pass through the wormhole. The motion starts at $r = 2.6$, the velocity decreases until the particle arrives near the throat after which it returns, moving away with increasing speed. In this case the particle stays on the same side of the wormhole and does not cross the throat.



(b) A particle starts its motion at $r = 2.6$, traverses the throat, and continues its motion with a growing absolute value of the velocity.

FIG. 16: Two different $\ell = 1$ geodesics for $\kappa = 0$, $L = \sqrt{1/10}$, $\omega = 0$, $\Lambda = 1.5$. We plot the motion with their corresponding E (right y-axis) and u^r (left y-axis) values.

VI. DISCUSSION AND CONCLUDING REMARKS

We have described how to construct new families of traversable wormhole solutions which are parametrized by a parameter ℓ , related to the angular momentum of the ghost fields supporting the throat, and discussed its effects on the shape of the geometric functions characterizing the solution, and on the geodesic motion of the corresponding spacetime. These families generalize previous wormhole spacetimes discussed in the literature [23, 24] which are recovered from our models by setting $\ell = 0$.

Indeed, we have obtained *bona fide* solutions to the Einstein-Klein-Gordon system and performed a detailed analysis of such solutions, which allowed us to gain a better understanding on the effects of the new parameter ℓ . We have been able to establish that its role on the geometric function a (determining the redshift factor), on the curvature scalars and on the density is quite similar to the role played by the frequency ω characterizing the time-dependency of the field, while its effect on these quantities is opposite to the one generated by the parameter of self-interaction Λ . Moreover, as can be clearly seen in the plot of the effective potential for time-like geodesics shown in Fig. 14, as the value of ℓ grows, the positions of the local minima move farther away from the throat, which is similar to the effect of increasing the angular momentum L of the test particles. In this sense, from the point of view of the test particle, the parameter ℓ plays a similar role than its conserved total angular momentum L .

It is interesting to point out that the energy density of some of our solutions – despite of the fact that the stress-energy-momentum violates the null energy condition – is actually positive close to the throat (but changes its sign as one moves away from it and then converges to zero which is consistent with our asymptotic flatness assumptions). In fact, the construction of a wormhole does not necessarily require measurements of a negative energy density made by

static observers, as already indicated in [3]. However, the fact that the null energy condition is violated at the throat implies that such observers also measure a “superluminal” energy flux. In general, the wormhole solutions discussed in this article possess a much richer structure than the simple, reflection-symmetric Bronnikov-Ellis wormholes, whose energy density is everywhere negative. In particular, the spacetimes discussed here exhibit a rich profile of bumps and wells in their curvature scalars whose precise shape depends on the values of ℓ as much as it does on the other parameters.

Indeed, we presented a detailed analysis of the role played by the several parameters in our wormhole solutions, namely the self-interaction term Λ , the oscillating frequency, ω , and the angular momentum parameter, ℓ of the scalar fields. Moreover, we have proved that there are no solutions for which the metric and scalar fields are reflection-symmetric about the throat if $\Lambda = 0$ (see Theorem 1). In this sense, the self-interaction term needs to be included in the action in order to extend the solution space. Actually, we have seen that it plays a smoothing role in the geometric reaction to the ghost matter. Also, we have seen that the effects on the geometry of the self-interaction parameter is opposite to the effects due to the frequency ω . As mentioned previously, the role of the ℓ parameter on the geometry is similar to the one generated by the frequency. This fact can be used to obtain real scalar field wormholes, with a new degree of freedom analogous to the case in which the solution space is extended by permitting the scalar field to be complex and harmonic in time. As shown in Theorem 2, all our wormhole solutions are characterized by a single throat whose areal radius is fixed by the parameters and the value of the scalar field at the throat, see Eq. (4.1).

We also provided a study of the effects of the parameters on the embedding diagrams visualizing the spatial geometry of the solutions, including the shape of the throat for several relevant cases. Finally, we presented a detailed analysis of the effective potential describing the motion of free-falling test particles as a function of the parameters, and we showed how the potential may present a local maximum at the throat which is surrounded by regions with local minima. Accordingly, we obtained several interesting types of trajectories. Depending on the values of the parameters and on those of the constants of motion (namely, the energy and angular momentum of the particle), we displayed trajectories approaching the throat until they reach a turning point and go back, other trajectories which describe bound motion on either side of the throat, and then we even obtained orbits that are bound but cross the throat repeatedly and keep passing from one side of the Universe to the other; a nice property for a space station!

In the plots of Fig. 16 we have shown the behavior of the geodesics passing through the throat, we presented the absolute value of the particle’s radial velocity and showed that it decreases as the particle approaches the throat until it crosses it after which it increases again as the particle gets further away from the throat. Such behavior is consistent with the interpretation that the reaction of the geometry to the ghost matter is to create bumps in the effective potential, instead of the wells generated by the usual matter. As mentioned at the beginning of Section II, there is no need to invoke negative masses to explain such behavior; it is simpler to imagine that the reaction of the geometry to the ghost matter is to create bumps that the particle have to surmount, consistent with the fact that the absolute value of the velocity decreases as it approaches the throat, and then, goes down the hill.

The new configurations we have found and discussed in this article considerably extend the parameter space describing wormhole solutions of the Einstein-scalar field equations, and they provide a large arena that offers the possibility to further study the intriguing properties of wormhole spacetimes, including the relation between the properties of exotic matter and their geometry. While it has been shown that the solutions with $\ell = 0$ are linearly unstable [23, 32, 35], there is hope that such a large arena may contain a set of parameter values with $\ell > 0$ describing stable wormholes or unstable wormholes with a very large timescale associated to their instability, a question that will be discussed in a future work.

Acknowledgments

We thank Fabrizio Canfora for pointing out to us the existence of traversable wormhole geometries in the absence of exotic matter. This work was partially supported by DGAPA-UNAM through grants IN110218 and IA101318 and by the CONACyT Network Project No. 294625 “Agujeros Negros y Ondas Gravitatorias”. This work has further been supported by the European Union’s Horizon 2020 research and innovation (RISE) program H2020-MSCA-RISE-2017 Grant No. FunFiCO-777740. BC and VJ acknowledge support from CONACyT. OS was partially supported by a CIC grant to Universidad Michoacana.

-
- [1] S. Krasnikov. A Traversable wormhole. *Phys. Rev.*, D62:084028, 2000. [Erratum: *Phys. Rev.*D76,109902(2007)].
- [2] M. Visser, S. Kar, and N. Dadhich. Traversable wormholes with arbitrarily small energy condition violations. *Phys. Rev. Lett.*, 90:201102, 2003.
- [3] F. S. N. Lobo. Energy conditions, traversable wormholes and dust shells. *Gen. Rel. Grav.*, 37:2023–2038, 2005.
- [4] F. S. N. Lobo. Phantom energy traversable wormholes. *Phys. Rev.*, D71:084011, 2005.
- [5] F. S. N. Lobo. Stability of phantom wormholes. *Phys. Rev.*, D71:124022, 2005.
- [6] J. L. Friedman, K. Schleich, and D. M. Witt. Topological censorship. *Phys. Rev. Lett.*, 71:1486–1489, 1993. [Erratum: *Phys. Rev. Lett.*75,1872(1995)].
- [7] C. Armendariz-Picon, V. F. Mukhanov, and P. J. Steinhardt. A Dynamical solution to the problem of a small cosmological constant and late time cosmic acceleration. *Phys. Rev. Lett.*, 85:4438–4441, 2000.
- [8] J. Garriga and A. Vilenkin. Solutions to the cosmological constant problems. *Phys. Rev.*, D64:023517, 2001.
- [9] D. Huterer and M. S. Turner. Probing the dark energy: Methods and strategies. *Phys. Rev.*, D64:123527, 2001.
- [10] E. J. Copeland, M. Sami, and S. Tsujikawa. Dynamics of dark energy. *Int. J. Mod. Phys.*, D15:1753–1936, 2006.
- [11] C. Escamilla-Rivera, R. Lazkoz, V. Salzano, and I. Sendra. Tension between SN and BAO: current status and future forecasts. *JCAP*, 1109:003, 2011.
- [12] E. A. Kazin et al. The WiggleZ Dark Energy Survey: improved distance measurements to $z = 1$ with reconstruction of the baryonic acoustic feature. *Mon. Not. Roy. Astron. Soc.*, 441(4):3524–3542, 2014.
- [13] Planck Collaboration. Planck 2013 results. XVI. Cosmological parameters. *A&A*, 571:A16, Nov 2014.
- [14] H. G. Ellis. Ether flow through a drainhole - a particle model in general relativity. *J. Math. Phys.*, 14:104–118, 1973.
- [15] K. A. Bronnikov. Scalar-tensor theory and scalar charge. *Acta Phys. Polon.*, B4:251–266, 1973.
- [16] F. Abe. Gravitational Microlensing by the Ellis Wormhole. *Astrophys. J.*, 725:787–793, 2010.
- [17] M. S. Morris and K. S. Thorne. Wormholes in space-time and their use for interstellar travel: A tool for teaching general relativity. *Am. J. Phys.*, 56:395–412, 1988.
- [18] F. S. N. Lobo. Exotic solutions in General Relativity: Traversable wormholes and 'warp drive' spacetimes. In *Classical and Quantum Gravity Research, 1-78, (2008), Nova Sci. Pub. ISBN 978-1-60456-366-5*. 2007.
- [19] M. Visser. *Lorentzian wormholes: From Einstein to Hawking*. 1995.
- [20] T. Matos and D. Nunez. Rotating scalar field wormhole. *Class. Quant. Grav.*, 23:4485–4496, 2006.
- [21] E. Teo. Rotating traversable wormholes. *Phys. Rev.*, D58:024014, 1998.
- [22] M. Alcubierre, J. Barranco, A. Bernal, J. C. Degollado, A. Diez-Tejedor, M. Megevand, D. Nunez, and O. Sarbach. ℓ -Boson stars. *Class. Quant. Grav.*, 35(19):19LT01, 2018.
- [23] V. Dzhunushaliev, V. Folomeev, B. Kleihaus, and J. Kunz. Wormhole solutions with a complex ghost scalar field and their instability. *Phys. Rev.*, D97(2):024002, 2018.
- [24] V. Dzhunushaliev, V. Folomeev, R. Myrzakulov, and D. Singleton. Non-singular solutions to Einstein-Klein-Gordon equations with a phantom scalar field. *JHEP*, 07:094, 2008.
- [25] P. Kanti, B. Kleihaus, and J. Kunz. Wormholes in Dilatonic Einstein-Gauss-Bonnet Theory. *Phys. Rev. Lett.*, 107:271101, 2011.
- [26] E. Ayon-Beato, F. Canfora, and J. Zanelli. Analytic self-gravitating Skyrmions, cosmological bounces and AdS wormholes. *Phys. Lett.*, B752:201–205, 2016.
- [27] M. Visser and C. Barcelo. Energy conditions and their cosmological implications. In *Proceedings, 3rd International Conference on Particle Physics and the Early Universe (COSMO 1999): Trieste, Italy, September 27-October 3, 1999*, pages 98–112, 2000.
- [28] E. Majerotto, D. Sapone, and L. Amendola. Supernovae Type Ia data favour negatively coupled phantom energy. *Submitted to: Phys. Rev. D*, 2004.
- [29] R. H. Price. Negative mass can be positively amusing. *American Journal of Physics*, 61(3):216–217, 1993.
- [30] I. Olabarrieta, J. F. Ventrella, M. W. Choptuik, and W. G. Unruh. Critical Behavior in the Gravitational Collapse of a Scalar Field with Angular Momentum in Spherical Symmetry. *Phys. Rev.*, D76:124014, 2007.
- [31] J. D. Jackson. *Classical Electrodynamics*. Wiley, 1998.
- [32] J. A. Gonzalez, F. S. Guzman, and O. Sarbach. Instability of wormholes supported by a ghost scalar field. I. Linear stability analysis. *Class. Quant. Grav.*, 26:015010, 2009.
- [33] S. L. Liebling and C. Palenzuela. Dynamical Boson Stars. *Living Rev. Rel.*, 15:6, 2012. [Living Rev. Rel.20,no.1,5(2017)].
- [34] C. W. Misner and D. H. Sharp. Relativistic equations for adiabatic, spherically symmetric gravitational collapse. *Phys. Rev.*, 136:B571–B576, 1964.
- [35] J. A. Gonzalez, F. S. Guzman, and O. Sarbach. Instability of wormholes supported by a ghost scalar field. II. Nonlinear evolution. *Class. Quant. Grav.*, 26:015011, 2009.